Controlling the electrostatic Coulomb interaction using metamaterials

Ilker Karakasoglu and Shanhui Fan

CONTROLLING ELECTROSTATIC COULOMB INTERACTION USING METAMATERIALS

Ilker Karakasoglu and Shanhui Fan

Department of Electrical Engineering,

Stanford University, Stanford, California 94305, United States

ABSTRACT

We study electrostatic screening in two classes of metamaterials. The first class consists of a cubic array of metal cubes, which is known to give rise to a positive local dielectric function. We show that such a local positive dielectric function also correctly describes its electrostatic behavior. The second class consists of a variety of wire media that have a strong nonlocal response in their dielectric function. We show that in these wire media, the electrostatic potential generated by a point charge decays exponentially as a function of distance from the charge, and such an exponential screening is intrinsically related to the nonlocal behavior of the dielectric function. We also show, surprisingly, that the electrostatic behavior in some of these wire media is isotropic in spite of the strong anisotropy in the dielectric tensor. Our work here provides an understanding of how to geometrically control electrostatic screening and Coulomb interaction in metamaterials.

I.INTRODUCTION

The dielectric function and the magnetic permeability were widely considered to be materials' intrinsic properties that cannot be easily engineered. The developments of metamaterials, however, allow geometric control of the dielectric function and the magnetic permeability, and have led to many new opportunities for controlling the propagations of electromagnetic waves [1] [2] [3] [4].

In addition to its importance in describing electromagnetic wave propagation, the dielectric function also controls the electrostatic screening. In vacuum, two static

charges separated by a distance interact through the Coulomb interaction. Inside a material, the Coulomb interaction between the two charges is reduced in its strength due to the electrostatic screening. The control of the Coulomb interaction and the electrostatic screening is of great interest for solid-state devices. As just one example, in excitonic solar cells such as organic and dye-sensitized solar cells, the ability to lower the Coulomb force via increasing the electrostatic screening facilitates exciton separation into electrons and holes and hence may be important for efficiency improvement [5]. The effect of electrostatic screening is described by the dielectric function. Since metamaterials allow geometric control of dielectric function, it is of fundamental importance to study how to design metamaterials to control electrostatic screening and Coulomb interaction. Such a study, however, has not been reported previously.

In free-electron metals, it is well known that the electrostatic limit where the frequency ω approaches zero needs to be carefully handled. While the electromagnetic wave properties of a free-electron metal can be well described by the Drude model which gives a local dielectric function that is negative below the plasma frequency, such a local dielectric function cannot be used at the $\omega \to 0$ limit to describe electrostatic screening [6]. Instead, the nonlocal aspects of the dielectric function, as described by the Thomas-Fermi approximation, are essential to provide a correct description of the electrostatic screening behavior [6].

Motivated by the consideration of the electrostatic screening in material systems, in this paper we study electrostatic screening in two classes of metamaterials. The first class consists of a cubic array of metal cubes, which is known to give rise to a local positive dielectric function. We show that such a local positive dielectric function also correctly describes its electrostatic behavior. The second class consists of a variety of wire media that have a strong nonlocal response in their dielectric function. We show that in these wire media, the electrostatic potential generated by a point charge decays exponentially as a function of distance from the charge, and such an exponential screening is intrinsically related to the nonlocal behavior of the dielectric function. We also show, surprisingly, that the electrostatic behavior in some of these wire media is

isotropic in spite of the strong anisotropy in the dielectric tensor. Our work here provides an understanding of how to geometrically control electrostatic screening and Coulomb interaction in metamaterials.

The rest of the paper is organized as following: In Sec. II, as a background, we briefly review the electrostatic screening in bulk metals to highlight the relevant aspects for subsequent discussions on metamaterials. In Sec. III, we describe various metamaterial structures and present the theoretical results on the electrostatic screening in these metamaterial structures using the appropriate dielectric functions. In Sec. IV, we validate the theoretical findings presented in Section III with direct numerical simulations of the metamaterial structures. Finally, we conclude in Section V.

II. SCREENING IN BULK METALS

Before investigating metamaterials in the electrostatic limit, we briefly review the electrostatic screening in bulk metals. In general, the electromagnetic properties of a metal is described by its dielectric function $\varepsilon(\omega, k)$, where k is the wavevector and ω is the angular frequency. For most studies of electromagnetic wave properties in metal, one assumes a local dielectric function: [6]

$$\varepsilon(\omega) \; = \; \varepsilon(\omega, k = 0) \; = \; \varepsilon_0 \left(1 - \frac{\omega_0^2}{\omega^2} \right)$$

(1)

where ε_0 is the dielectric constant of the free space, and ω_0 is the plasma frequency. Eq. (1) provides a description of the plasmonic behavior of metal. On the other hand, to treat dielectric screening at the electrostatic limit, the nonlocal behavior of the dielectric function is essential. At $\omega=0$, the Thomas-Fermi approximation gives:

$$\varepsilon(\omega = 0, k) = \varepsilon_0 \left(1 + \frac{k_s^2}{k^2} \right)$$

(2)

where k_s is the Thomas-Fermi wavevector. From Eq. (2), we can express the electric potential φ associated with a point charge q placed in metal as

$$\varphi(k) = \frac{q}{\varepsilon_0} \frac{1}{k^2 + k_s^2}.$$

(3)

Taking the inverse Fourier transform of $\varphi(k)$, we obtain the screened electric potential:

$$\varphi(r) = \frac{q}{4\pi\varepsilon_0} \frac{e^{-k_s r}}{r}.$$

(4)

As seen in this brief review above, the electrostatic screening is controlled by the nonlocal dielectric function in the electrostatic limit $\varepsilon(0, k)$. Metamaterials have generated substantial excitements due to the possibility of engineering dielectric functions that are not available in naturally occurring materials. Unlike the control of electromagnetic waves, however, to control electrostatic screening with metamaterials, one needs to focus on the nonlocal response. With this consideration in mind, in the next section we discuss various metamaterial systems.

III. METAMATERIALS IN THE ELECTROSTATIC LIMIT

In this section, we study the electrostatic characteristics of metamaterials theoretically by considering the effective dielectric tensors of these materials. The theoretical prediction here will then be checked against direct numerical simulations in Section IV. We examine five different topologies of metamaterials: one is a cubic array of metal cubes (Fig. 1) and the other four are wire media consisting of metallic wires (Figs. 2-5). These metamaterial structures are chosen to highlight those structural aspects that are important to control the electrostatic screening.

In all metamaterials considered in this section, the metals are assumed to be perfect electric conductors (PEC) and embedded in a uniform lossless dielectric host medium, which is assumed, without any loss of generality, to be the vacuum with the

electric permittivity ε_0. As will be shown in Sec. B, without loss of generality any metal can be used instead of PEC. In the electrostatic regime, plasmonic losses do not have any impact on the Coulomb interaction. Having stated the common factors in all metamaterials, we now introduce each one separately.

A. Cubic array

The first metamaterial we consider is a cubic array of metal cubes as illustrated in Fig. 1. The lattice constant is *a* and the size of a cube is *b*.
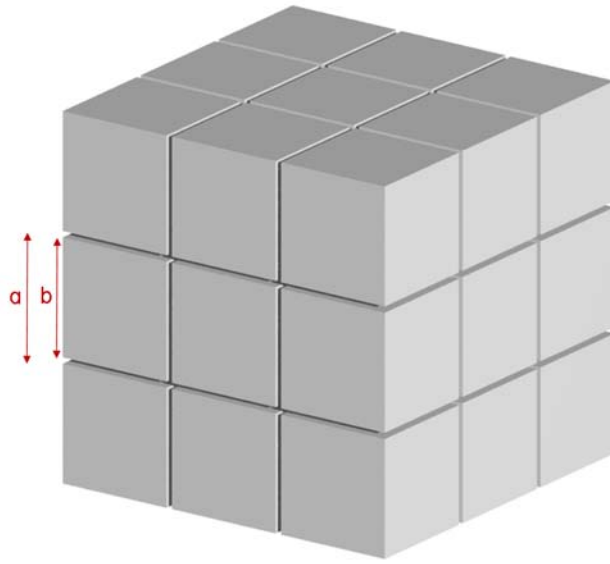

FIG. 1. A cubic array composed of isolated metal cubes. (a: lattice constant, b: length of a side of a cube)

The relative dielectric function ε_r of a cubic array can be found by a local homogenezation model [7]. Since this topology has an octahedral (Oh) symmetry point group, its electromagnetic properties are isotropic with ε_r being a scalar [8] [9]. In the large cube limit (i.e., b ≈ a), ε_r is approximated as [10]

$$\overline{\quad\quad}$$

$$\tag{5}$$

Using this dielectric model, the electric potential of point charge q in a cubic array is given by

$$\rule{3cm}{0.4pt} \quad -$$

<div align="right">(6)</div>

B. Uniaxial wire medium

Fig. 2 shows a uniaxial wire medium, which consists of a two-dimensional square array of parallel infinitely long thin wires. The lattice constant of the square array is a. We denote the radius of wires as r_0. The radius r_0 is assumed to be much smaller than the lattice spacing a (r_0<<a).
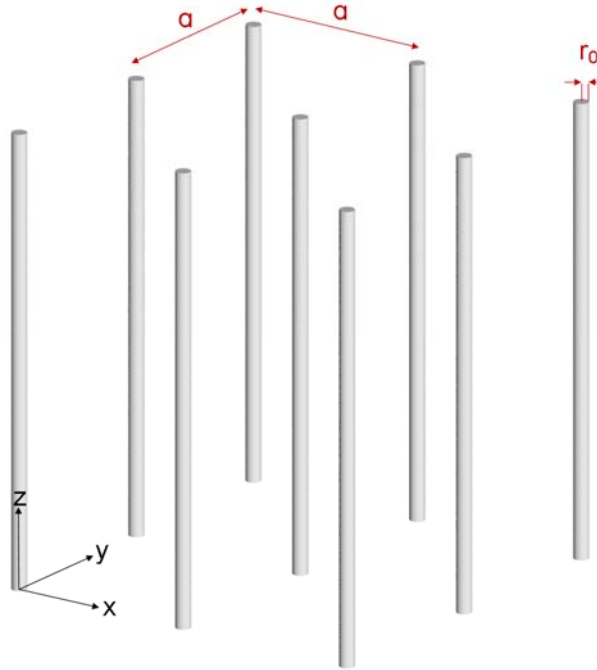

FIG. 2. The geometry of a uniaxial wire medium formed by infinitely long PEC wires arranged in a square lattice. (a: lattice constant, r_0: wire radius)

Unlike cubic arrays of metal cubes as shown in Fig. 1, wire media have prominent nonlocal effects [11] [12] [13] [14]. In the presence of spatial dispersion, the electric displacement vector **D** and the magnetic field **H** at a point of space can no longer be written in terms of average electric field **E** and average induction field **B** at the same point of space. Instead, they can be related in the Fourier domain by a nonlocal dielectric function _____. As it was shown, this dielectric function alone is sufficient to

describe the homogenized medium [15] [16]. The nonlocal dielectric function can be derived analytically using the thin wire assumption, i.e., $r_0/a \ll 1$. With this assumption, polarizations due to the metal-wire that are orthogonal to wires are negligible. Thus, the effective permittivity for an external electric-field polarized orthogonal to wires is simply the host medium permittivity ε_0. Therefore, a uniaxial wire medium (Fig. 2) can be modelled using the following permittivity dyadic:

$$\overline{\overline{\varepsilon}}(\beta, k) = \varepsilon_0 (\mathbf{x}_0 \mathbf{x}_0 + \mathbf{y}_0 \mathbf{y}_0 + \varepsilon_z(\beta, k_z) \mathbf{z}_0 \mathbf{z}_0)$$

(7)

where x_0, y_0 and z_0 are unit vectors directed along the respective direction. $\beta = \omega\sqrt{\varepsilon_0\mu_0}$ is the wavenumber corresponding to ω in the host medium. The wavevector k is given by $(k_x, k_y, k_z)^T$, where k_x, k_y and k_z refer to the wavevector components in respective directions x, y or z. A nonlocal dispersive model was developed for ε_z as [11] [12]

$$\varepsilon_z(\beta, k_z) = 1 - \frac{\beta_0^2}{\beta^2 - k_z^2}.$$

(8)

Here, as a good analytic approximation, β_0 is given by [11] [14]

$$\beta_0^2 = \frac{2\pi/a^2}{\ln\left(\frac{a}{2\pi r_0}\right) + 0.5275}.$$

(9)

which is solely defined by the medium's geometry parameters a and r_0. Here, it should be noted that $\varepsilon_z(\beta, k_z)$ can be generalized to include plasmonic losses [17] [18]:$\varepsilon_z(\beta, k_z) = 1 + \dfrac{1}{\dfrac{1}{(\varepsilon_{metal}-1)f_V} - \dfrac{\beta^2 - k_z^2}{\beta_0^2}}$

(10)

where $f_V = \pi(r_0/a)^2$ is the volume fraction of wires and ε_{metal} is the dielectric function of metal used in wires, which is given by the Drude model and is complex. For the

electrostatic case ω=0, Eq. 8 is recovered from Eq. 10. Thus, in the electrostatic case metal loss does not play a role. In general, while metals have a non-zero conductivity at ω=0, there is no electric current inside metals in the case we consider in the paper, and hence there is no loss. This argument applies to all other geometries that we consider in this paper.

We use the dielectric function of Eqs. (8) and (9) to discuss the electrostatic screening. For the electrostatic analysis, we can take the β→0 limit of $\varepsilon_z(\beta,k_z)$ to obtain:

$$\varepsilon_z(0,k_z) = 1 + \frac{\beta_0^2}{k_z^2},$$

(11)

and therefore $\bar{\bar{\varepsilon}}(\beta,k)$ becomes

$$\frac{\bar{\bar{\varepsilon}}(0,k)}{\varepsilon_0} = \mathbf{x}_0\mathbf{x}_0 + \mathbf{y}_0\mathbf{y}_0 + (1 + \frac{\beta_0^2}{k_z^2})\mathbf{z}_0\mathbf{z}_0.$$

(12)

Having the dielectric function expressed in the electrostatic limit, we can determine the electric potential of a point charge q placed in this medium using Gauss's law:

$$\nabla \cdot \mathbf{D}(r) = \frac{q}{\varepsilon_0}.$$

(13)

In the k-space, the electric displacement field **D** is related to the electric field **E** by $\mathbf{D}(k) = \bar{\bar{\varepsilon}}(0,k)$ **E**(k). Additionally, using the relation **E**(r) = - ∇φ and converting this relation into the k-space, we can re-write Eq. (12) as

$$(-ik)\bar{\bar{\varepsilon}}(k)\,(-ik)\varphi(k) = -\frac{q}{\varepsilon_0}.$$

(14)

And as a result, φ(k) is found to be:

$$\varphi(k) = \frac{q}{\varepsilon_0} \frac{1}{k^2 + \beta_0^2}.$$

(15)

In real space, the electric potential is then:

$$\varphi(r) = \frac{q}{4\pi\varepsilon_0} \frac{e^{-\beta_0 r}}{r}.$$

(16)

The functional form of φ(k) and φ(r) given by Eq. (15) and Eq. (16) are the same as those for bulk metals (given by Eq. (3) and Eq. (4)). Like in bulk metals, we can define, for this uniaxial wire medium, a screening length: $1/\beta_0$. Unlike in bulk metals, however, where the screening length is controlled entirely by material properties, in these metamaterials the screening length is controlled by geometry. Therefore, it becomes possible to control the Coulomb interaction by engineering the geometry of the medium.

Also, remarkably, while the dielectric tensor for such a uniaxial wire medium (Eq. (11)) is strongly anisotropic, the resulting electrostatic potential (Eq. (15)) is completely isotropic in space. We will see such elimination of anisotropy is in fact quite general for other wire medium as well.

C. Biaxial wire medium

Figure 3 shows a biaxial wire medium. It consists of two sets of doubly periodic wires oriented along two orthogonal directions (z- and y- directions, respectively). Each set of the wires forms a square lattice with a lattice constant a. The wires do not intersect, and the axes of adjacent orthogonal wires are spaced by a/2.
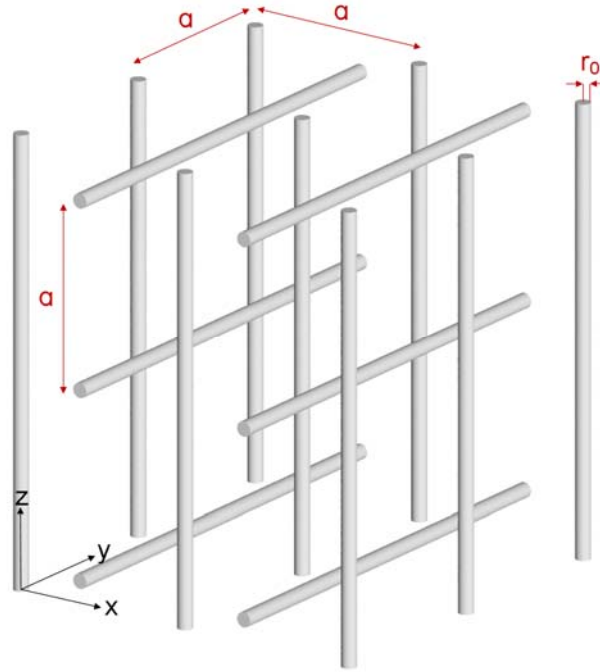
FIG. 3. The geometry of a biaxial wire medium formed by two sets of mutually orthogonal infinitely long PEC wires, each set arranged in square lattices. (a: lattice constant, r_0: wire radius)

As the starting point of the derivation of electric potential, we use a general dielectric function formalism— similar to the one in Eq. (8) for a uniaxial wire medium. For a biaxial wire medium,   reads [13]

$$(17)$$

where

$$(18)$$

$$(19)$$

Such separation of $\bar{\bar{\varepsilon}}(\beta, k)$ into its components $\varepsilon_y(\beta, k_y)$ and $\varepsilon_z(\beta, k_z)$ rests on the assumption that the polarizations from orthogonal wires do not interact with each other. Therefore, $\varepsilon_y(\beta, k_y)$ can independently be derived like $\varepsilon_z(\beta, k_z)$ given in Eq. (8). $\varepsilon_y(\beta, k_y)$ and $\varepsilon_z(\beta, k_z)$ have the same form as required by the symmetry of the structure.

Having $\bar{\bar{\varepsilon}}(\beta, k)$ derived, we can examine the electrostatic limit. For $\beta \to 0$, $\bar{\bar{\varepsilon}}(\beta, k)$ approaches

$$\frac{\bar{\bar{\varepsilon}}(0, k)}{\varepsilon_0} = \mathbf{x_0 x_0} + \left(1 + \frac{\beta_0^2}{k_y^2}\right) \mathbf{y_0 y_0} + \left(1 + \frac{\beta_0^2}{k_z^2}\right) \mathbf{z_0 z_0}.$$

(20)

Solving Poisson's Equation with this $\bar{\bar{\varepsilon}}(0, k)$, $\varphi(k)$ and $\varphi(r)$ are found to be

$$\varphi(k) = \frac{q}{\varepsilon_0} \frac{1}{k^2 + 2\beta_0^2},$$

(21)

$$\varphi(r) = \frac{q}{4\pi\varepsilon_0} \frac{e^{-\sqrt{2}\beta_0 r}}{r}$$

(22)

where the screening length is $1/(\sqrt{2}\beta_0)$. Here, again we see the same effect as the uniaxial wire medium case of an isotropic electrostatic response from a highly anisotropic dielectric tensor.

D. Triaxial wire media

Having three sets of wires, with the sets being orthogonal to one another, we obtain a triaxial wire medium. Again, each set of wires has a square lattice of a lattice constant a. We consider two different configurations of triaxial media: nonconnected

and connected, which are depicted in Fig. 4 and Fig. 5, respectively. While the nonconnected medium has mutually orthogonal adjacent wires separated by a/2, the connected medium has intersecting wires.
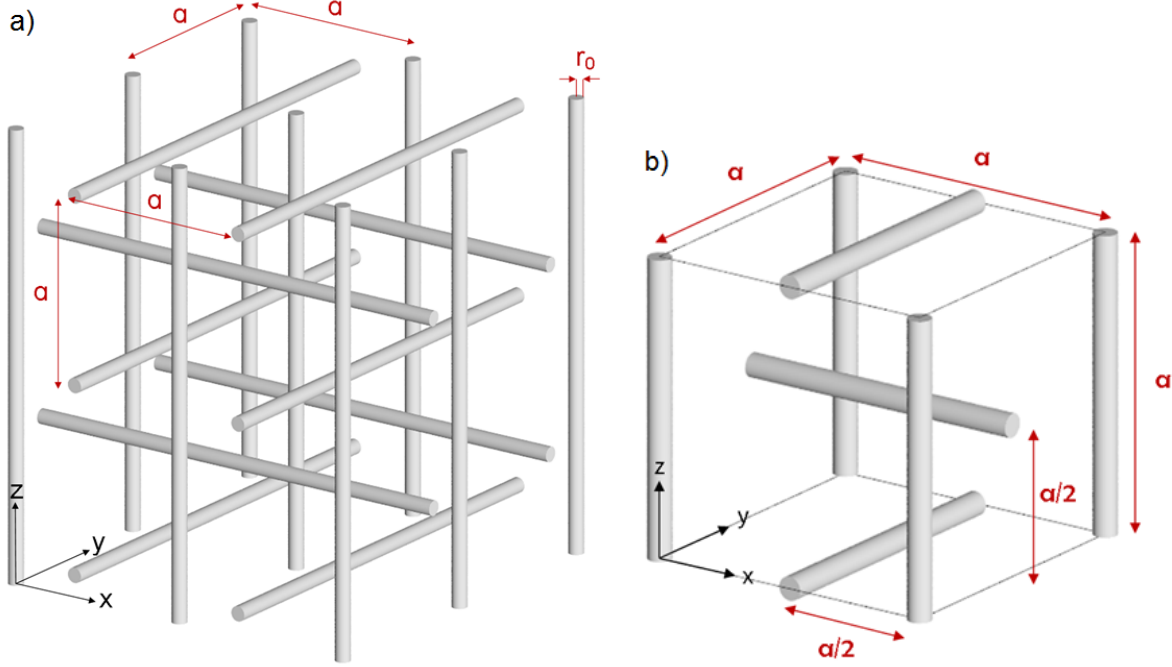

FIG. 4. The geometry of a nonconnected triaxial wire medium formed by three sets of mutually orthogonal infinitely long PEC wires arranged in square lattices (adjacent orthogonal wires are spaced of a/2). (a: lattice constant, r_0: wire radius). (a) Multiple periodicities. (b) A single unit cell

Due to their different connectivity, these two media have different electrostatic characteristics. The derivation of the electric potential in a nonconnected triaxial medium follows the same pattern of a biaxial medium. $\overline{\overline{\varepsilon}}(\beta, k)$ has the general form of

$$\overline{\overline{\varepsilon}}(\beta, k) = \varepsilon_0\left(\varepsilon_x(\beta, k_x)\mathbf{x}_0\mathbf{x}_0 + \varepsilon_y(\beta, k_y)\mathbf{y}_0\mathbf{y}_0 + \varepsilon_z(\beta, k_z)\mathbf{z}_0\mathbf{z}_0 \right).$$

(23)

Based on the same assumptions as discussed above for biaxial medium, $\overline{\overline{\varepsilon}}(\beta, k)$ for the triaxial non-connected wire medium is [14]

$$\frac{\overline{\overline{\varepsilon}}(\beta, k)}{\varepsilon_0} = \overline{\overline{I}} - \frac{\beta_0^2}{\beta^2 - k_x^2}\mathbf{x}_0\mathbf{x}_0 - \frac{\beta_0^2}{\beta^2 - k_y^2}\mathbf{y}_0\mathbf{y}_0 - \frac{\beta_0^2}{\beta^2 - k_z^2}\mathbf{z}_0\mathbf{z}_0$$

(24)

where $\overline{\overline{I}}$ is a unit dyadic. In the electrostatic limit ($\beta \to 0$), $\overline{\overline{\varepsilon}}(\beta, k)$ becomes

$$\frac{\overline{\overline{\varepsilon}}(0, k)}{\varepsilon_0} = \overline{\overline{I}} + \frac{\beta_0^2}{k_x^2}\mathbf{x}_0\mathbf{x}_0 + \frac{\beta_0^2}{k_y^2}\mathbf{y}_0\mathbf{y}_0 + \frac{\beta_0^2}{k_z^2}\mathbf{z}_0\mathbf{z}_0.$$

(25)

Using this $\overline{\overline{\varepsilon}}(0, k)$ to solve Poisson's Equation, we find $\varphi(k)$ and $\varphi(r)$ as

$$\varphi(k) = \frac{q}{\varepsilon_0}\frac{1}{k^2 + 3\beta_0^2}$$

(26)

$$\varphi(r) = \frac{q}{4\pi\varepsilon_0}\frac{e^{-\sqrt{3}\beta_0 r}}{r}$$

(27)

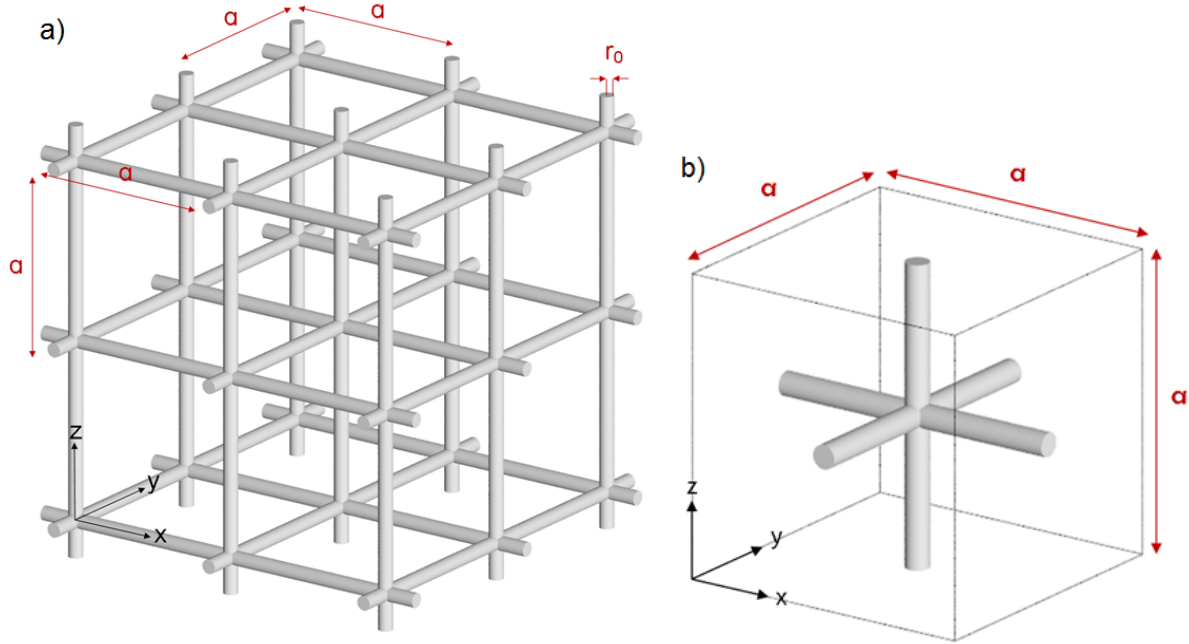where the screening length is $1/(\sqrt{3}\beta_0)$.

FIG. 5. The geometry of a connected triaxial wire medium formed by three sets of mutually orthogonal infinitely long PEC wires arranged in a square lattice. (a: lattice constant, r_0: wire radius). (a) Multiple periodicities. (b) A single unit cell

A connected medium is formed by three mutually orthogonal sets of wires joined at the intersection points (Fig. 5). Unlike in a nonconnected medium, here the polarizations in the different sets of the wires do couple to each other. As a result, $\bar{\bar{\varepsilon}}(\beta, k)$ takes the form [14] [19]

$$\frac{\bar{\bar{\varepsilon}}(\beta, k)}{\varepsilon_0} = \bar{\bar{I}} - \frac{\beta_0^2}{\beta^2}\left(\bar{\bar{I}} - \frac{\mathbf{kk}}{k^2 - l_0\beta^2}\right)$$

$$l_0 = \frac{3}{1 + 2\frac{\beta_0^2}{\beta_1^2}}$$

(28)

where β_1 is another medium geometry dependent variable and is given by [14]

$$\frac{1}{\beta_1^2} = \left(\frac{a}{2\pi}\right)^2 \sum_{l \neq 0} \frac{\left[J_0\left(\frac{2\pi l r_0}{a}\right)\right]^2}{l^2}.$$

Here, l is an integer and J_0 stands for the Bessel function of the first kind and order 0. Limit $\beta \to 0$ cannot directly be applied on this $\overline{\overline{\varepsilon}}(\beta, k)$ because $\overline{\overline{\varepsilon}}(0, k)$ diverges to negative infinity. However, the electrostatic screening is controlled only by the longitudinal part of the dielectric function, we therefore decompose $\overline{\overline{\varepsilon}}(\beta, k)$ into its longitudinal ε_l and transverse ε_t components:

$$\frac{\overline{\overline{\varepsilon}}(\beta, k)}{\varepsilon_0} = \varepsilon_t(\beta)\left(\overline{\overline{I}} - \frac{\mathbf{kk}}{k^2}\right) + \varepsilon_l(\beta, k)\left(\frac{\mathbf{kk}}{k^2}\right)$$

(30)

where

$$\varepsilon_t(\beta) = 1 - \frac{\beta_0^2}{\beta^2},$$

(31)

$$\varepsilon_l(\beta, k) = 1 + \frac{l_0\beta_0^2}{k^2 - l_0\beta^2}.$$

(32)

Such decomposition in Eq. (29) is possible since the connected triaxial medium has a cubic symmetry [15] . For $\beta \to 0$, ε_l reads

$$\varepsilon_l(0, k) = 1 + \frac{l_0\beta_0^2}{k^2}.$$

(33)

Solving Poisson's Equation with this $\varepsilon_l(0,k)$, we find the electric potential as

$$\varphi(k) = \frac{q}{\varepsilon_0}\frac{1}{k^2 + l_0\beta_0^2},$$

(34)

$$\varphi(r) = \frac{q}{4\pi\varepsilon_0}\frac{e^{-\sqrt{l_0}\beta_0 r}}{r}$$

(35)

where the screening length is $1/(\sqrt{l_0}\beta_0)$.

To summarize Section III, we see that all presented wire media create exponentially decaying isotropic electric potentials. Since these structures have different connectivity properties, the theoretical results indicate that it is the nonlocal aspects of the dielectric function which arises from the infinite nature of the wires, rather than the connectivity properties, that lead to the exponential screen behavior. For the wire media considered here, the difference between their electrostatic properties is their strength of screening, as characterized by screening lengths. Screening lengths are found as $1/(\beta_0)$, $1/(\sqrt{2}\beta_0)$, $1/(\sqrt{3}\beta_0)$ and $1/(\sqrt{l_0}\beta_0)$ for a uniaxial, biaxial, nonconnected triaxial and connected triaxial, respectively.

We emphasize that the effective dielectric functions that have been assumed in this section have all been previously developed to account for the properties of electromagnetic waves with non-zero frequencies. Whether these dielectric functions can be used to account for the electrostatic properties of these systems have in fact never been tested before. This is not a trivial issue. As we have seen in Section II, the commonly used dielectric function of Eq. (1) does give excellent description of the electromagnetic properties of free-electron metal, but it gives qualitatively incorrect prediction of the electrostatic screening in metal when one takes the $\omega\rightarrow 0$ limit. Therefore, in the next section we provide direct numerical calculations of the electrostatic screen in the metamaterial systems described above in order to confirm the theoretical prediction provided here.

V. NUMERICAL RESULTS

Our numerical approach involves solving Poisson's Equation for the electric potential distribution $\varphi(r)$ for physical structures. A commercial software package (Sentaurus TCAD) [20] is used to perform the simulations. The simulation domain

includes a finite-size metamaterial structure with several periods in all three dimensions. The finite-size structure is surrounded by air regions. A point test charge q is placed in the origin of the simulation space, which is also the center of the metamaterial structure. In order to account for the electric potential approaching zero in infinity in real space, a Dirichlet boundary condition of $\varphi(r=\text{boundary})=0$ is imposed on the outer boundary of the simulation domain. No boundary condition for $\varphi(r)$ is applied on the metal surfaces, i.e., on cubes and wires. Instead, charge neutrality is imposed on each metal structure. The electrostatic potential of each metal element is determined in the simulation from this charge neutrality condition.

Initially, we perform a control simulation of the empty space. We obtain $1/(\varepsilon_0 r)$ dependence of the electric potential as expected. We use this electric potential as a reference for comparisons in the subsequent metametarial simulations. Since the studied metamaterials theoretically have infinite dimensions, large dimensions for the simulation space need to be chosen. We find that a simulation domain with a size of 12a x 12a x 12a gives sufficiently accurate results.

The first simulated metamaterial is the cubic array of metal cubes (Fig. 1). For the unit cell size a and the cube side length b, we choose the geometry as b = 19/20a. We present simulation results in two forms as illustrated in Fig. 6. $\varphi(r)$ vs r is plotted in Fig. 6(a), and $\ln(r\,\varphi(r))$, where ln is the natural logarithm, vs r is plotted in Fig. 6(b). The use of $\ln(r\varphi(r))$ provides a simple graphic means to distinguish between the 1/r and the $e^{-\kappa r}/r$ dependency with respect to r, where $1/\kappa$ denotes the screening length. With $\ln(r\,\varphi(r))$ as the vertical axis, the 1/r dependency would be a flat line while the $e^{-\kappa r}/r$ dependency would be represented by a straight line whose slope is the negative inverse of the screening length, i.e., $-\kappa$. As expected, we observe a flat line in Fig. 6(b). By comparing it to the electric potential curve associated with the empty space, we see that the electric potential in a cubic array is lower due the enhanced ε_r. Therefore, the local dielectric function of Eq. (5) provides an accurate description of the electrostatic properties of such a metamaterial consisting of a cubic array of metal cubes.
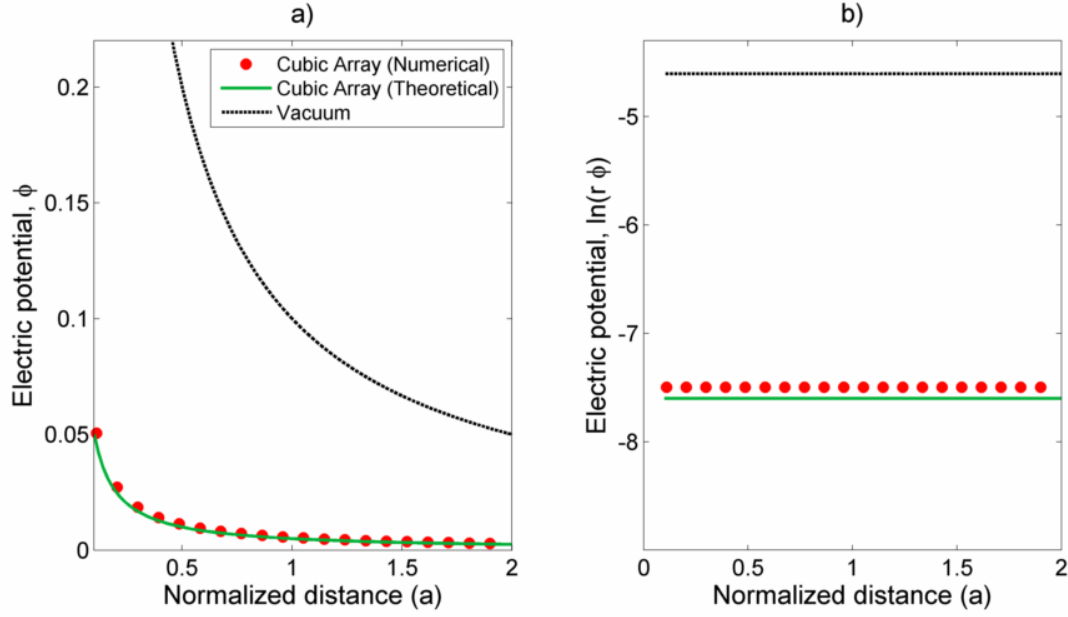
FIG. 6. Electric potential as a function of distance normalized by the lattice constant a for a single point charge placed in a cubic array compared to electric potential in vacuum: (a) Electric potential. (b) Transformed electric potential. The transformation is done by multiplying the electric potential by distance and taking the natural logarithm of this multiplication. As expected, flat lines are observed both for vacuum and a cubic array because electric potentials have 1/r dependency. The lower flat line of the cubic array is due to the enhanced relative dielectric function.

We next simulate the wire media illustrated in Figs. 2-5. We choose the radius of the wires $r_0 = 1 \times 10^{-3}a$, in order to satisfy the condition for the thin-wire approximation ($r_0 \ll a$). When displaying the simulation results of the electric potential, we use $\ln(r\, \varphi(r))$ as the vertical axis. The results demonstrated in Fig. 7 show that $\ln(r\, \varphi(r))$ scales linearly with respect to r with a negative slope, thus electric potentials $\varphi(r)$ indeed decay exponentially in wire media.
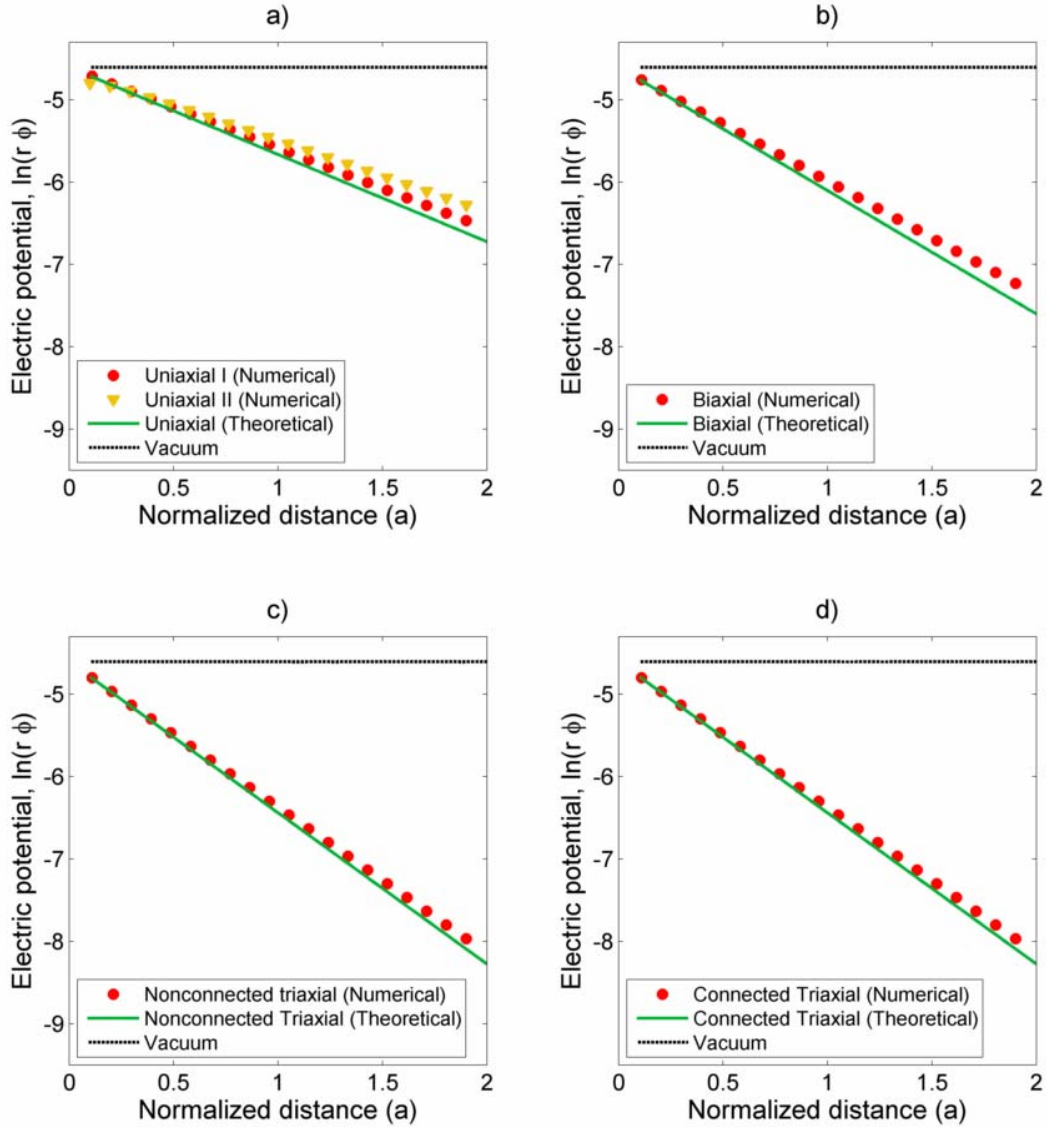
FIG. 7. Transformed electric potential as a function of distance normalized by the lattice constant a for a single point charge placed in (a) uniaxial, (b) biaxial, (c) nonconnected triaxial and (d) connected triaxial wire media. The electric potential in vacuum is given as a reference for comparison. The transformation of electric potential is done by multiplying it by distance and taking the natural logarithm of this multiplication. The electric potential in vacuum results in a flat line because this electric potential has 1/r dependency. On the contrary, transformed electric potentials drop linearly, which is an indication of exponential decay in un-transformed electric potentials. Slopes of lines show how strong exponential decays are. In (a), a pair of numerical results is illustrated: (I) and (II). (II) shows the electric potential along a direction perpendicular to uniaxial wires, whereas (I) shows the electric potential in a direction parallel to wires.

Such a discrepancy occurs due to numerical reasons. Theoretically, electric potential shall fall off isotopically.

In order to understand how well theoretical and numerical results agree, we compare theoretical and numerical screening lengths. The theoretical ones are calculated as $1/\beta_0 = 0.943a$, $1/(\sqrt{2}\beta_0) = 0.667a$, $1/(\sqrt{3}\beta_0) = 0.544a$, and $1/(\sqrt{l_0}\beta_0) = 0.544a$ for a uniaxial medium, a biaxial medium, a nonconnected triaxial medium and a connected triaxial medium, respectively. Numerical screening lengths of wire media are obtained by taking the negative inverse of slopes of $\ln(r\,\varphi(r))$ lines. For all systems, theoretical and numerical results agree well as seen in Figure 7. For the simulation of the empty space, there is ~1% difference between the numerical and the theoretical one. For the simulations of metamaterials, we observe a difference of about 10% between theoretical and numerical results. This error is associated with the limited dimensions of the simulation space. Increasing the number of units cells of metametarials used, we observe monotonically decreasing discrepancies between the theoretical results and the numerical simulations.
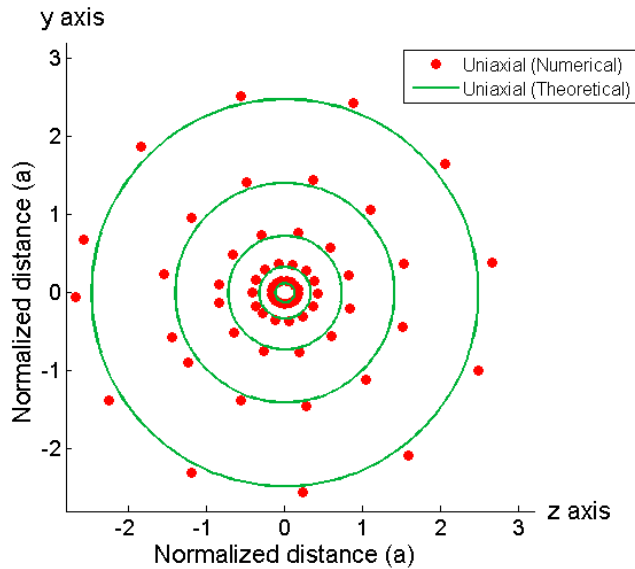

FIG. 8. Equipotential lines in the y-z plane of a single point charge placed in a uniaxial wire medium. Wires are along the z axis. The theoretical expectation is perfectly circular equipotentials. Numerical results generally agree with the theoretical expectation, the small discrepancy is due to imperfect numerical convergence.

In the simulation of the uniaxial medium, as a function of r, the electric potential parallel to the axis of wires is approximately equal to the electric potentials in orthogonal directions (as seen in Fig. 7(a) and Fig. 8). The slight discrepancy of the electric potentials along these two directions occurs due to the finite size of the simulation space. Making the space larger reduces the discrepancy. In a biaxial medium, there is no observable difference for the electric potentials along the direction parallel to a set of wires, and along the direction orthogonal to all wires (Fig 7b). The numerical results here confirm that for both the uniaxial and the biaxial wire media, the electrostatic properties of the structure is isotropic in spite of the strong anisotropy of the dielectric tensors. To summarize this section, the numerical results provide an excellent confirmation of the theoretical results as presented in Section III.

VI. CONCLUSION

In this paper, we have analyzed theoretically the electrostatic characteristics of two classes of metamaterials. The first class consists of a cubic array of metal cubes. We show that its electrostatic screening behavior can be described by a positive local dielectric function. In such a system, the electrostatic potential from a static charge scales as $1/(\varepsilon_r r)$, where the ε_r is the effective dielectric constant of the metamaterial, and r is the distance from the charge. The second class consists of a variety of wire media. In these systems, we show that the electrostatic potential from a static charge scales as $\exp(-\kappa r)/r$, where $1/\kappa$ is the screening length. We also show that such an exponential behavior is intrinsically related to the nonlocal nature of the effective dielectric model. The theoretical analysis is confirmed by direct numerical simulations of the metamaterial structures.

In both classes the metamaterials, the properties of the electrostatic screening, such as the effective dielectric constant in the first class, and the screening length in the second class, are directly related to the geometrical parameters of the metamaterial structures. Therefore, we have shown that metamaterials offer geometrical control of the Coulomb interaction. Given the importance of the Coulomb interaction both in fundamental physics and in device applications, our work points to a new potential area of applications for metamaterials, which have not been extensively explored before.

ACKNOWLEDGEMENTS

References

1) J. B. Pendry, Phys. Rev. Lett. 85, 3966 (2000).

2) R. A. Shelby, D. R. Smith and S. Schultz, Science 292, 5514 (2001).

3) D. R. Smith, J. B. Pendry, and M. C. K. Wiltshire, Science 305, 788 (2004).

4) N. I. Landy, S. Sajuyigbe, J. J. Mock, D. R. Smith, and W. J. Padilla, Phys. Rev. Lett. 100, 207402 (2008).

5) B. A. Gregg, J. Phys. Chem. B 107, 4688-4698 (2003).

6) C. Kittel, Introduction to Solid State Physics. John WIley and Sons. 8th ed (2005).

7) J. B. Pendry, A. J. Holden, D. J. Robbins, and W. J. Stewart, IEEE Trans. Microwave Theory Tech. 47, 2075 (1999).

8) V. M. Agranovich and V. L. Ginzburg, Crystal Optics with Spatial Dispersion and Excitons (Springer-Verlag, Berlin, 1984).

9) P. Halevi and F. Perez-Rodriguez, Proc. SPIE Int. Soc. Opt. Eng. 6320, 63200T (2006).

10) J. Shin, J. Shen, and S. Fan, Phys. Rev. Lett. 102, 093903 (2009).

11) P. A. Belov, S. Tretyakov, and A. Viitanen, J. Electromagn. Waves Appl. 16, 1153 (2002).

12) P. A. Belov, R. Marques, S. I. Maslovski, I. S. Nefedov, M. Silveirinha, C. R. Simovski, and S. A. Tretyakov, Phys. Rev. B 67, 113103 (2003).

13) C. R. Simovski and P. A. Belov, Phys. Rev. B 70, 046616 (2004).

14) M. G. Silveirinha and C. A. Fernandes, IEEE Trans. Microw. Theory Tech. 53, 1418 (2005).

15) L. D. Landau and E. M. Lifshitz, Electrodynamics of Continuous Media, Course of Theoretical Physics (Elsevier, New York, 2004), Vol. 8, p. 360.

16) M. G. Silveirinha, Phys. Rev. B 75,115104 (2007).

17) M. G. Silveirinha, Phys. Rev. E 73, 046612 (2006).

18) M. G. Silveirinha, C. A. Fernandes and J. R. Costa, IEEE Trans. Ant. and Prop. 56, 2 (2008).

19) S. I. Maslovski and M. G. Silveirinha, Phys. Rev. B 80, 245101 (2009).

20) Sentaurus, TCAD. Synopsys. Inc., Z-2012.03 edition (2012).